Chapter 3

MOCVD Growth of Electrically Conductive AlGaN/GaN Distributed Bragg Reflectors with High Reflectivity

3.1 Introduction

III-V nitride semiconductors are quite promising materials especially for short-wavelength optoelectronic device applications. Among such devices, Nitride-based blue-violet vertical-cavity surface-emitting lasers (VCSELs) have received great attention because of their various advantages. For example, two-dimensionally integrated short-wavelength laser arrays can emit parallel beams, which will significantly increase data transfer rate of high-density optical data storage system such as Blu-ray Disc (BD) or HD-DVD. Since the first unambiguous demonstration of optically pumped lasing of nitride VCSELs at room temperature [16], various efforts have been devoted to realize current injection operation in VCSELs and vertical microcavity LEDs (MCLEDs). Many groups have reported growth of nitride DBRs[18, 63-81]. However, one of the most difficult issues has been to grow electrically conductive nitride DBRs with high reflectivity.

In this chapter, MOCVD growth of electrically conductive AlGaN/GaN DBRs is discussed. Structural, optical and electrical properties of the DBRs are studied systematically. From Si doping concentration dependence of structural and optical properties of n-DBRs, it can be concluded that reasonable reflectivity can be maintained with uniform carrier concentration profile of 1×10^{18} cm^{-3}. The author shows that the carrier concentration in n-AlGaN layers can be increased up to 3×10^{18} cm^{-3} while that of n-GaN is kept at constant value, 1×10^{18} cm^{-3}, without further degradation of

optical properties. Using such modulated doping profiles, electrical properties of the n-DBRs can be improved. As a result, it is possible to obtain near 99 % reflectivity in electrically conductive n-type nitride DBRs. Further improvement in both structural and electrical characteristics can be achieved by introducing n-AlGaN/n-GaN short-period superlattice into the n-DBRs. Theoretical studies on potential profiles and electrical conductivity of nitride n-DBRs are also presented.

3.2   Growth of III-Nitride Distributed Bragg Reflectors by Atmospheric Pressure Metalorganic Chemical Vapor Deposition

All samples were grown on c-axis-oriented sapphire substrates by atmospheric pressure metalorganic chemical vapor deposition (MOCVD). Trimethylaluminum (TMA) and trimethylgallium (TMG) were used as group III precursors, while ammonia was used as a nitrogen source. Carrier gases used were both H_2 and N_2. Donor and acceptor doping were performed using monosilane and bis-(cycropentadienyl)magnesium as n-type and p-type dopant sources, respectively. Substrates used in this research was commercially available c-face sapphire supplied by Kyocera. Dimensions of the substrate is 21 mm × 16 mm × 0.33 mm. The substrate was set on a graphite susceptor coated with SiC. In order to suppress turbulence and to obtain homogenous epilayers near the substrate edges, dummy substrates were located surrounding the substrate.

The schematic diagram of growth sequence for nitride DBR is presented in the previous chapter (Fig. 2.2). At first, the substrate was heated up to 930 °C at the ramping rate of 150 °C/min and then was hold at the temperature for 4 min under constant NH_3 flow of 0.5 slm (standard litter per minutes). During this stage, surface of the sapphire substrate was cleaned and nitridated. After the cleaning, the substrate was cooled down to around 480 °C, where the low-temperature GaN buffer layer was deposited on the substrate. Flow rates of the sources for the LT-GaN growth was 22 μmol/min and 3.5 slm for TMG and NH_3, respectively. Only H_2 carrier gas was introduced with flow rate of 16 slm during the growth. The growth rate of the LT-GaN was approximately 17 nm/min and 140-sec growth resulted in a 40-nm-thick LT-GaN layer. Then, the substrate was heated again up to around 1071 °C with ramping rate of 210 °C/min, and GaN layer growth was initiated on the deposited and annealed LT-GaN buffer. Flow rates of the sources and carrier gases for the HT-GaN growth was 88 μmol/min, 4.0 slm, 4.0 slm and 11.5 slm for TMG, NH_3, H_2, and N_2, respectively. The growth rate of the HT-GaN under this condition was approximately 25 nm/min. Total thickness of the two GaN buffer layers was set at $5/4\lambda$ (~192 nm). Then the sample

was heated up to around 1092 °C without interrupting source supply. Thereafter, flow rate of N_2 carrier gases were increased to 28.0 slm, resulting increased velocity of the sources. This condition effectively suppress parasitic reactions in the gas phases between NH_3 and TMA. Quarter-wavelength AlGaN and GaN layers were stacked on the GaN buffer. $Al_xGa_{1-x}N$ layers were grown with various TMA flow rates in order to control Al composition x. Typically, using TMA and TMG flow rates of 27 μmol/min and 16 μmol/min with 4.0 slm NH_3 flow, approximately 40 % Al composition can be obtained. Growth rate of GaN with total carrier flow rate of 32.0 slm was decreased to 15 nm/min. Growth rate of the AlGaN layer was 3.8 nm/min with above-mentioned conditions. When the whole DBR structure was grown, supply of the metalorganics were halted and RF heater was off. NH_3 flow was stopped after the substrate was cooled below 500 °C. The sample was brought out from the reactor after cooling and evaluated optically or structurally.

Optical and structural characterization of the grown DBRs were performed both at room temperature. Reflectivity of the DBRs were measured by using Xe lump as a light source. A reference aluminum mirror of which reflectivity was known was used to normalize the reflected spectra taken from the DBRs. In addition, a high-reflectivity multi-coated dielectric mirror which have the stop-band around 400 nm was used to precisely calibrate the peak reflectivity of high-reflectivity samples. High-resolution x-ray diffraction (HRXRD) measurements were done with the Philips X'Pert-MRD double-crystal x-ray diffractometer system using $CuK\alpha_1$ radiation.

3.3   Si Doping into AlGaN/GaN Distributed Bragg Reflectors

There have been several proposals to realize nitride VCSEL or microcavity devices. In such proposals, Song et al. utilized metal mirror instead of dielectric or semiconductor DBRs [19]. In this case, process procedure must be complex and difficult because of epitaxial lift-off process used to separate epitaxial films from their substrate. In addition, a metal mirror is insufficient in terms of reflectivity for VCSEL applications. Diagne et al. have proposed microcavity using insulating nitride DBRs [70]. In order to inject carriers into active regions, one must precisely control etching depth to access n-GaN, which is the lower half of the microcavity itself. To achieve reasonable yields, the thickness of the n-GaN layer must have relatively thick such that etching can be stopped properly at the layer. The thinner the cavity is, the more dominantly the microcavity effects occur since the effective mode volume inversely proportional to the Purcell enhancement factor is also reduced. From this point of view, their approach using insulating DBRs has its own limitation. If

25

one can use electrically conductive, high reflectivity nitride DBRs instead of above-mentioned structures such as metal or insulating mirrors, it is obvious that process margins will be increased. For this purpose, we have grown Si-doped AlGaN/GaN DBRs, which is described in this section.

3.3.1 Doping Concentration Dependence

In order to investigate doping dependence on DBR characteristics, 15-period AlGaN/GaN DBRs with various uniform doping concentrations in both GaN and AlGaN have been grown. Atomic force microscopy (AFM) was used to investigate surface morphologies of the DBRs. As Si doping concentration increased, larger roughness was observed. At maximum doping levels studied (apporx. 1×10^{19} cm^{-3}), there appeared large (~100 nm in diameter) pits on the surface. Reflectivity also depends on Si doping concentration, as shown in Fig.3.1. Almost 10 % decrease in reflectivity was observed when carrier density reached 5×10^{18} cm^{-3}. X-ray diffraction also reflects the crystalline quality of the DBRs. When Si doping concentration increased, satellite fringes became less visible. On the other hand, negligible degradation was observed not only in XRD but also in reflectivity measurements when the concentration was kept at 1×10^{18} cm^{-3}.

Doped impurities induce optical loss or absorption in DBR. Because GaN has smaller bandgap than AlGaN, the effect of dopant is much more dominant in GaN than in AlGaN. Nakwaski et al theoretically investigated and designed nitride VCSELs [82]. One must carefully design absorption of the materials to practically minimize its influences. VCSELs require very little absorption, or the threshold current density drastically increases.

3.3.2 Total Thickness Dependence

With a doping concentration fixed to 5×10^{17} cm^{-3}, we have grown n-AlGaN/n-GaN DBRs with different thickness in order to investigate thickness dependence of structural characteristics. Optical microscope and AFM measurements revealed that there was no crack and smooth surface could be obtained in spite of highly strained structure. Figure 3.2 shows thickness dependence of optical reflectivity. Despite their relatively high doping concentration, almost the same reflectivity as nondoped DBRs can be grown. It was further confirmed that thicker n-DBRs up to 35-period can be grown without any critical degradation.
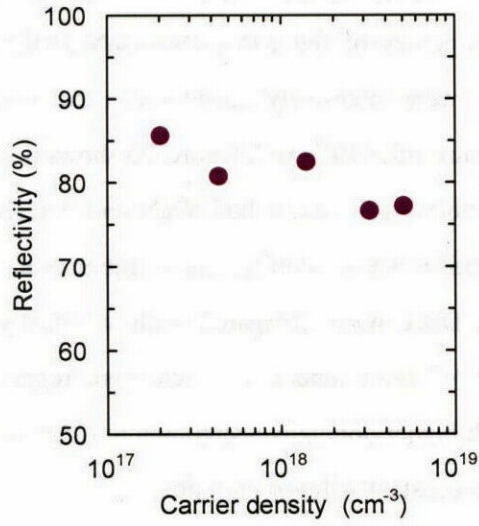
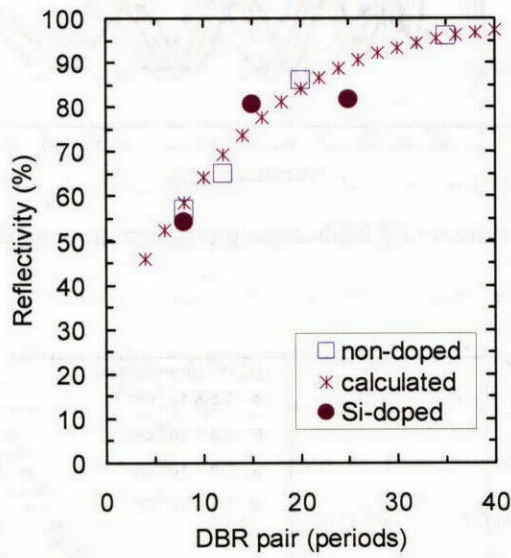Figure 3.1 Si doping dependence of reflectivity of AlGaN/GaN DBR

Figure 3.2 DBR total thickness dependence of reflectivity of n-AlGaN/n-GaN DBRs

3.3.3 Improvement of Electrical Properties by Intense Doping into AlGaN

To improve electrical properties of the n-AlGaN/n-GaN DBRs maintaining good optical quality, only n-AlGaN layers were intensively doped while the donor concentration in n-GaN layers was kept at a constant value of 1×10^{18} cm^{-3}. Figure 3.3 shows n-AlGaN doping concentration dependence of reflectivity. Unlike as the cases both GaN and AlGaN were equivalently doped, reflectivity did not degrade until n-AlGaN doping concentration reached as high as 3×10^{18} cm^{-3}. Electrical properties of this DBR were compared with constantly-doped DBRs, measuring current-voltage characteristics of p-i-n junctions which were regrown on the DBRs. Fig 3.4 illustrates the I-V curves. With higher doping concentration in n-AlGaN layers, the modified DBR exhibited lower resistance than constantly-doped ones do.
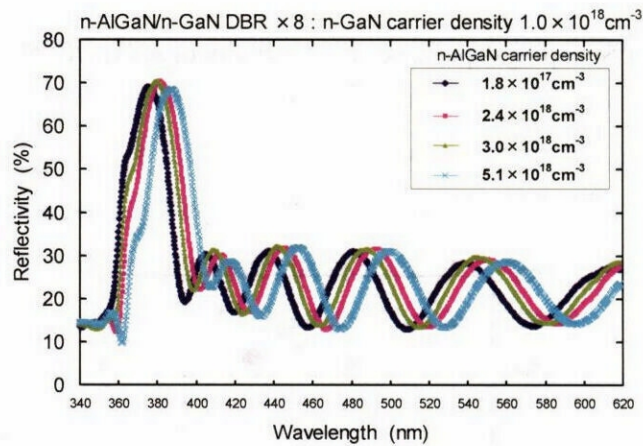
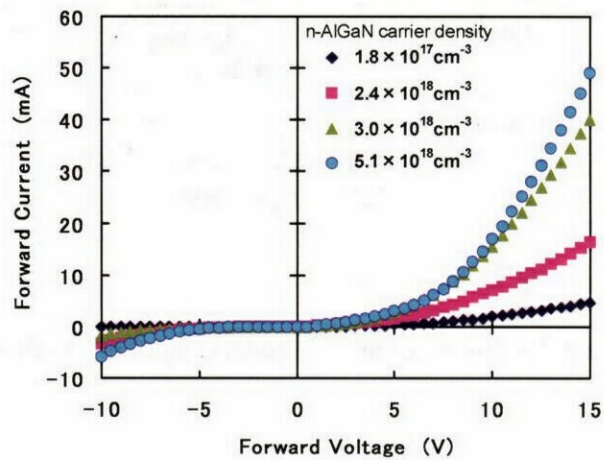Figure 3.3 Effects of AlGaN doping concentration on reflectivity

Figure 3.4 Effects of AlGaN doping concentration on electrical properties of AlGaN/GaN DBRs

3.4 Introduction of AlGaN/GaN Superlattices

Although Si-doped n-AlGaN/n-GaN DBRs were successfully grown and current injection through the nitride n-DBR has been achieved as will be described in detail in chapter 5, further improvements of electrical, optical and structural properties are required in order to realize nitride VCSELs. For this purpose, we propose n-AlGaN/n-GaN superlattice DBRs (SL-DBRs) in which n-AlGaN/n-GaN short-period superlattices are used instead of n-AlGaN quarter-wave layers in conventional DBRs. Recently, Y.-K. Su et al. reported that a tunneling effect in AlAs/[GaAs/AlAs] superlattice DBRs could be used to reduce electrical resistance of VCSELs [83]. Tunneling current flowing across appropriately designed superlattices may reduce resistance also in nitride VCSELs. In addition, though several groups have reported conductive AlGaN with high Al concentration [84], such conductive AlGaN is not easy to obtain. Alternatively, short-period superlattices are now widely used as cladding layers in nitride-based edge-emitting laser diodes. In the latter case, superlattices can improve conductivity of the cladding layers with relatively high average Al content, avoiding structural degradation. Similar effects are expected in the SL-DBR. In this section, we present growth and characterization results of the AlGaN/GaN superlattice DBR in detail.

3.4.1 Effects of AlGaN/GaN Superlattices on Strain

At first, in order to evaluate the efficacy of superlattices on stress engineering, a 10-period n-$Al_{0.50}Ga_{0.50}N$/n-GaN superlattice have been grown. Following a thermal cleaning sequence at 930 °C, a 30-nm-thick low-temperature GaN buffer was deposited on the sapphire substrate at around 460 °C. A 1.5-μm-thick nondoped GaN layer was then grown at 1071 °C. At this stage, the flow rate of TMG was set to 88 μmol/min while those of NH_3, N_2, and H_2 gases were 4.0, 11.5, and 4.0 slm, respectively. Then the superlattice was grown at 1102 °C. The $Al_{0.50}Ga_{0.50}N$ layers were grown with the flow rates of TMG and TMA fixed at flow rates of 16 and 38 μmol/min, respectively, while that of TMG was 44 μmol/min when both n-type and nondoped GaN layers were grown. During the growth of the superlattice, NH_3, H_2 and N_2 gases were constantly supplied at flow rates of 4.0, 4.0, and 28.0 slm, respectively. For a comparison, a n-$Al_{0.40}Ga_{0.60}N$ thin film has also been deposited at 1092 °C on another 1.5-μm-thick GaN with flow rates of 16 and 28 μmol/min for TMG and TMA, respectively. Both samples were doped with Si. The flow rates of SiH_4 (10 ppm) for n-$Al_xGa_{1-x}N$ (x = 0.5, 0.4) and n-GaN were 1.8 and 1.0 standard cubic centimeters per minute (sccm), respectively.

From the HRXRD measurements, the thicknesses of each n-Al$_{0.50}$Ga$_{0.50}$N layer and n-GaN layer in the superlattice were estimated to be 2.56nm and 0.64nm, respectively. The thickness of the n-Al$_{0.40}$Ga$_{0.60}$N film was measured to be 34.0nm. In Figure 3.5, the surface morphology images of these two samples taken with Nomarski optical microscope were shown. As shown in Figure 3.5, cracking was completely suppressed in the superlattice sample in spite of the fact that both samples had almost equivalent Al mole fraction and similar thickness in total. Although the critical thickness of AlGaN grown on GaN is still under discussion, observed cracks in the n-Al$_{0.40}$Ga$_{0.60}$N film were rather dense which may imply that the thickness of this film was not just above the critical thickness but considerably thicker than it. As explained by Einfeldt et al., edge cracks nucleated at the surface are assumed to propagate toward the GaN buffer before crack channeling starts [85]. It is possible that there were some barriers preventing crack to propagate across the superlattice which may be similar ones also mentioned by Einfeldt et al.
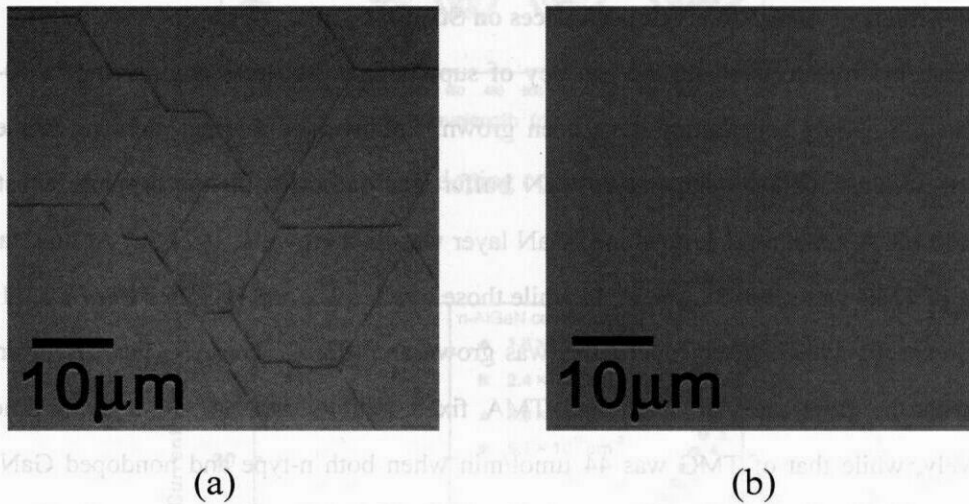

(a)   (b)

Figure 3.5 Optical Microscope images of (a) Al$_{0.4}$Ga$_{0.6}$N and (b) Al$_{0.5}$Ga$_{0.5}$N/GaN superlattice

3.4.2 Characterization of Superlattice DBRs

Next, a 26-pair SL-DBR was grown and characterized. Schematic structure of the SL-DBR is depicted in Figure 3.6. Superlattice inside the SL-DBR consisted of 16-period $Al_{0.44}Ga_{0.56}N(8ML)/GaN(2ML)$. An additional 38.0-nm-thick GaN layer completed the single pair of the DBR. During the growth of the $Al_{0.44}Ga_{0.56}N$ layers inside the SL-DBR, the flow rates of TMG and TMA were fixed at 16 and 32 μmol/min, respectively. For the purpose of fabricating MCLEDs on this SL-DBR, topmost 8-pair $[(Al_{0.44}Ga_{0.56}N)_8/(GaN)_2]_{16}/GaN$ layers were doped with Si. The flow rates of SiH_4 for n-$Al_{0.44}G_{0.56}N$ and n-GaN were 1.8 and 1.0 sccm, respectively. From independent Hall measurements, carrier concentration in the n-$Al_{0.44}Ga_{0.56}N$ and the n-GaN were estimated to be 3×10^{18} cm^{-3} and 1×10^{18} cm^{-3}, respectively. Other conditions such as growth temperature were the same as those of the above-mentioned superlattice. With these conditions, the growth rates of $Al_{0.44}Ga_{0.56}N$ and GaN were 2.7 nm/min and 17nm/min, respectively. NH_3, H_2 and N_2 gases were constantly supplied during the growth at flow rates of 4.0, 4.0, and 28.0 slm, respectively. Note that the total gas flow rate is almost two times faster than the standard condition for GaN buffer growth (NH_3 = 4.0 slm, H_2 = 4.0 slm, N_2 = 11.5 slm). When the total flow rate of the carrier gases are increased, constant supply rate of the precursors results in more dilute material gas mixture per unit volume of the whole gas. Roughly, all species involved in the MOCVD growth tend to stay at their equilibrium vapor pressures, hence the reduced vapor pressure for each material gas enhances desorption of atoms from the growing surface. Consequently, the growth rate becomes slower when the flow rates of carrier gases are increased. Empirically, a slow growth rate is effective for obtaining flat interfaces in AlGaN/GaN DBRs. It is important to suppress the parasitic reactions between TMA and NH_3 in the gas phase to grow relatively high Al-content AlGaN uniformly. The fast flow of material gases also effectively suppresses the undesirable reactions. Relatively thin, 260-nm-thick GaN buffers were used for these DBRs instead of a 1.5-μm-thick GaN buffer. As explained below, such a thin buffer makes it possible that whole DBR structure grow psuedomorphically.
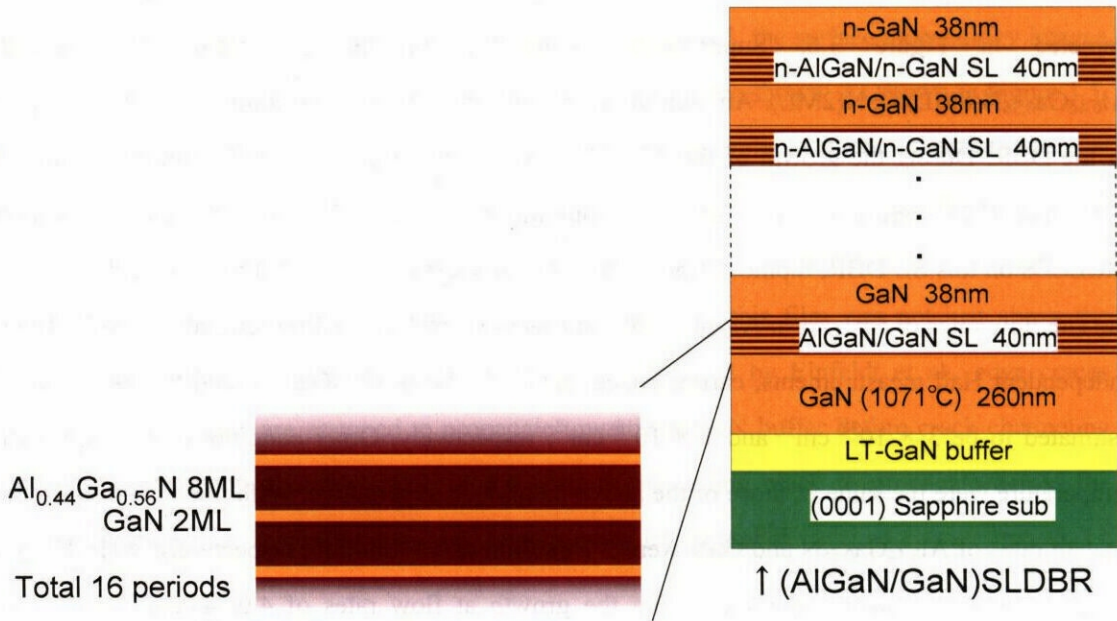
Figure 3.6 Schematic of fabricated [AlGaN/GaN]/GaN superlattice DBR

Figures 3.7 and 3.8 show HRXRD measurement results of the fabricated SL-DBR. In Fig. 3.7, an ω-2θ scan is plotted. There appear clear satellite peaks came from the short-period superlattice structure, indicating that abrupt interfaces and good uniformity can be obtained in it. Al composition in AlGaN layers and thicknesses of the constituent layers are derived from the simulation of the scan. Figure 3.8 shows a reciprocal space mapping result of the SL-DBR measured around (11-24) reflection. As can be seen, the GaN buffer layer and the whole superlattice DBR layers are grown almost pseudomorphically, i.e., the in-plane lattice constants of each layer are almost identical. It should be noted that the total thickness of the SL-DBR structure without the GaN buffer was thicker than 2.0 μm. Because strains seemed to be balanced inside the whole epitaxial layers, the 260-nm-thick GaN buffer itself was, presumably, compressively strained. Misfit dislocations generated at the interface between low-temperature GaN and the GaN buffer

layer may, to some extent, relief the stress during the DBR growth. Surface morphology observation revealed that cracking has been suppressed comparing with conventional DBRs that have almost equivalent Al content in AlGaN quarter-wave layers. Although the strain within AlGaN/GaN DBRs can be relaxed partially by a thin GaN buffer in general, superlattice in this SL-DBR possibly contributed to toughen the DBR layers against the crack. Nakada et al. reported that the insertion of an AlGaN/GaN superlattice prior to the growth of an AlGaN/GaN DBR could suppress cracking and improve reflectivity of the DBR [86]. In their results, the superlattice seems to have functioned as an intentional strain relaxation layer rather than a barrier preventing crack propagation.
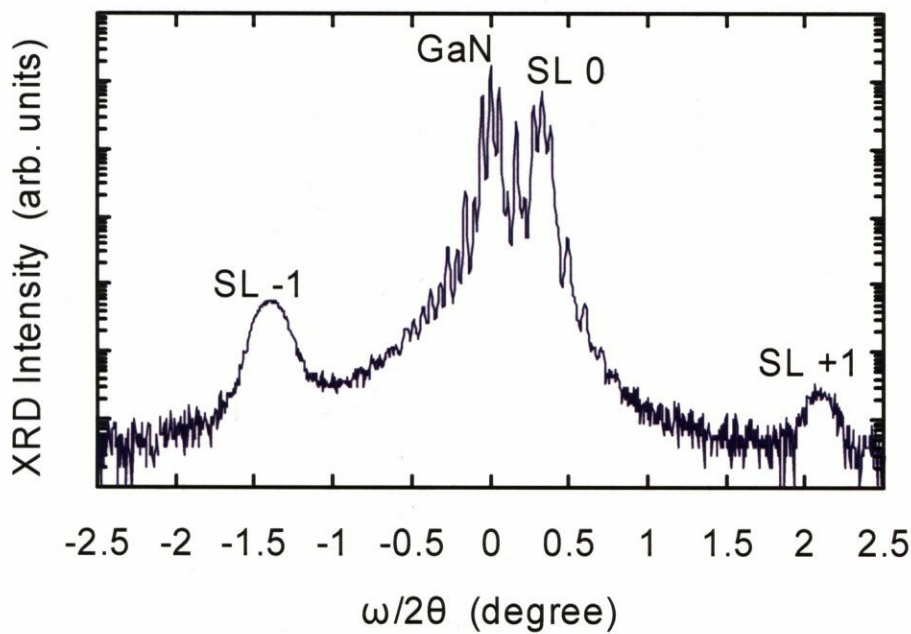

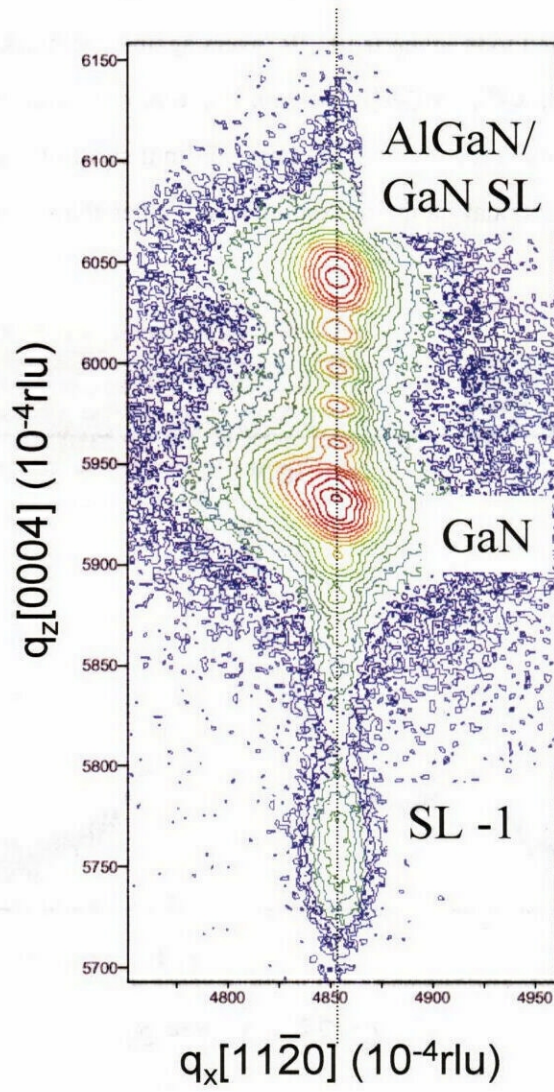
Figure 3.7 XRD scan of fabricated superlattice DBR

Figure 3.8 [11-24] reciprocal space map of the fabricated superlattice DBR

The SL-DBR was revealed to have peak reflectivity of 94.5 % at 401 nm, as shown in Figure 3.9. Numerical simulations using standard transfer-matrix method, with refractive indices for $Al_xGa_{1-x}N$ calculated from a literature, predicted that both superlattice-based and conventional DBRs had almost the same reflectivity when their total Al contents were equivalent. The superlattice with period well below the optical wavelength can be considered as a single layer for light waves. Measured reflectivity as high as those of conventional DBRs were in good agreement with the simulated result. Considering that higher Al content than conventional DBRs with similar structural quality are expected in the case of SL-DBR, one can also expect that even higher reflectivity than conventional DBRs can be obtained by utilizing superlattices. Similar DBR structure consisted of [AlN/GaN]SL/GaN was reported by Schenk et al [87]. They obtained reflectivity of 68 % at 444 nm with a 10-pair SL-DBR grown on Si(111) substrate. Although rather different conditions between their experiments and ours make it impossible to simply compare both results, we have successfully achieved much higher reflectivity with SL-DBR.
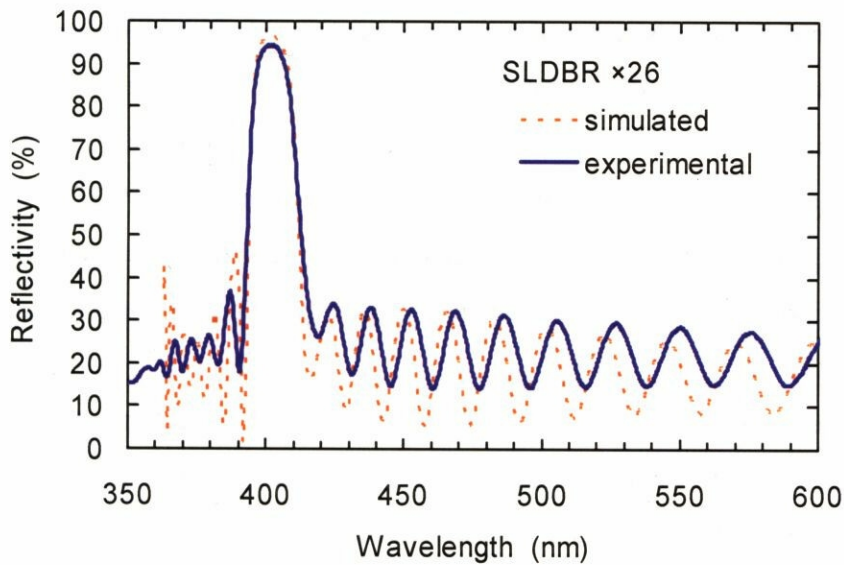

Figure 3.9 Reflectivity spectrum of a superlattice DBR

3.5 High Reflectivity III-Nitride DBRs for Nitride VCSELs

To obtain high reflectivity in DBRs, in general one must increase the number of DBR stacks or increase the refractive index difference between two constituents. A VCSEL requires very high reflectivity for the DBRs. Since the volume of its active region is too small, light have to propagate many times up and down inside the vertical cavity, in order to attain enough material gain to reach threshold. In AlGaAs/GaAs system, lattice mismatch between AlGaAs and GaAs is so negligible that it is not very difficult to obtain high reflectivity DBR by increasing stacking periods. On the other hand, III-nitrides usually suffer from serious strain problems which easily results in cracking especially when total thickness of the heteroepitaxial layers increases. So far, there have been several reports on high reflectivity nitride DBRs. Ng et al. reported 99% AlN/GaN DBR grown by MBE [88]. Although highest index contrast is available with these two binary compounds, strain prevents one to grow a high quality thick structure. Furthermore, even if such structure is grown, there remains another issue on electrical characteristics due to inherent difficulties to obtain efficient conductivity in large band-gap materials such as AlN. Ive et al insists that they can achieve both high reflectivity and conductive Si-doped AlN/GaN DBRs, in which interface states play important roles to obtain conductivity, according to their claims [89]. Further examination is necessary to conclude what is responsible for the unusual conductivity they have observed. Yet growth difficulty, partly explicated by the fact that all AlN/GaN DBRs reported were grown by MBE instead of MOCVD, makes DBRs with high Al-content AlGaN less attractive. Recently Carlin et al. reports over 99% reflectivity AlInN/GaN DBR grown by MOCVD [66]. Their approach is unique. AlInN with In content of 18% is considered to be perfectly lattice-matched to GaN. Designed appropriately, one can expect pseudomorphic growth within whole structure of the AlInN/GaN DBR [66, 67].

Here we present our results on high reflectivity AlGaN/GaN DBR growth. Approximately 99% reflectivity was obtained with 42-period $Al_{0.4}Ga_{0.6}N$/GaN DBR, in which topmost 9 periods were doped with Si. Epitaxial growth was done with MOCVD, as described in the previous section. In order to overcome cracking problems, we developed novel techniques to prevent the wafer edge regions of thick, strained AlGaN/GaN layers originate cracks. Details on the technology will be described in the next chapter. As shown in Fig. 3.10, reflectivity of the 42-period DBR was measured to be approximately 99 %.
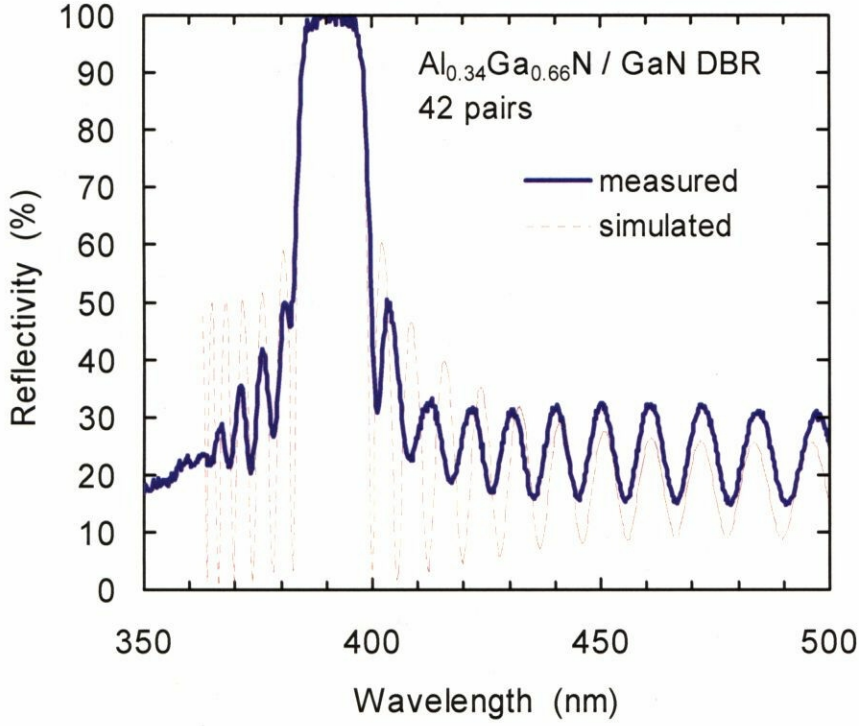
Figure 3.10 Reflectivity of a 42-period AlGaN/GaN DBR

A distributed Bragg reflector is one kind of mirrors. In DBRs, specific designated wavelength is reflected efficiently due to optical interferences. DBRs basically consist of alternate stacks of two different materials with different optical indices of refraction. Generally, optical thicknesses (optical path) d of each material (refractive index n) are designed to be a quarter of the designated wavelength λ. In other words, the thickness d is given as follows:

$$d = \frac{\lambda}{4n} \tag{3.1}$$

Peak reflectivity R of DBR consisted by N-pairs of two absorption-free, isotropic materials with refractive indices n_1 and n_2 is given as follows:

$$R = \left(\frac{\left(-\frac{n_2}{n_1}\right)^N - \frac{n_s}{n_0}\left(-\frac{n_1}{n_2}\right)^N}{\left(-\frac{n_2}{n_1}\right)^N + \frac{n_s}{n_0}\left(-\frac{n_1}{n_2}\right)^N} \right)^2 \tag{3.2}$$

Advances in semiconductor crystal growth technologies enable us to construct semiconductor DBRs in which semiconductor thin films are stacked. In particular, sufficiently high-quality DBRs can be obtained using nearly lattice-matching GaAs/AlAs system which also provides reasonable contrast of refractive indices. As can be seen from equation (2), the larger index contrast is, the less pairs of DBR are necessary to obtain high reflectivity. Simultaneously, wide stop-band width can also be obtained with large index contrast.

Optical constants of III-nitride semiconductors are theoretically and experimentally investigated so far, and Brunner et al. have given the following relation for $Al_{1-x}Ga_xN$ alloys from absorption measurements [90]:

$$n^2(hv, x) = C(x) + A(x)y^{-2}\left[2 - \sqrt{1+y} - \sqrt{1-y}\right] \tag{3.3}$$

where

$$\begin{aligned}
A(x) &= (3.17 \pm 0.39)x^{2/3} + (9.98 \pm 0.27) \\
C(x) &= -(2.2 \pm 0.2)x + (2.66 \pm 0.12) \\
y &= hv/E_g(x)
\end{aligned} \tag{3.4}$$

$E(g)$ is the bandgap energy of $Al_{1-x}Ga_xN$ at room temperature, hv means photon energy. Using these equations, reflectivity of nitride DBRs are calculated by transfer matrix method. Figure 3.11 shows two examples of the calculated reflectivity. 42-periods $Al_{0.35}Ga_{0.65}N$ (41nm) / GaN (38.4nm) DBR will give 99.5% reflectivity at the stopband center, 392 nm.

Relatively low contrast of refractive index and inherent strain between AlN and GaN (approximately 2.5%) causes severe problems such as cracking. In order to avoid cracking, one needs lower AlN content, resulting lower index contrast between AlGaN alloy and GaN. For example, refractive indices of $Al_{0.4}Ga_{0.6}N$ and GaN at 400 nm are 2.35 and 2.54, respectively, which in turn provide lower index contrast than other III-V materials such as GaAs/AlAs. Therefore relatively thicker stack of DBRs is necessary to obtain high reflectivity enough for the VCSEL applications. Fabrication of nitride VCSELs then becomes much more difficult.
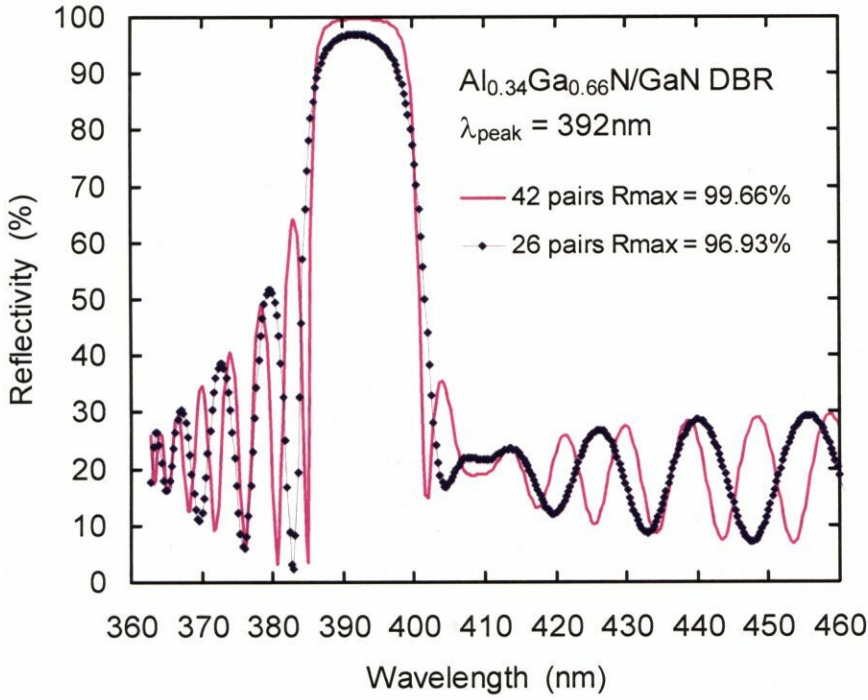
Figure 3.11 Simulated reflectivities of $Al_{0.34}Ga_{0.66}N/GaN$ DBRs with different periods

There must be smooth interfaces in the DBRs, or reflectivity degrades. Interface roughness can be approximately included into the standard transfer matrix method by taking into account the roughness parameter σ, the root mean square roughness of the interface. Assumption is made that lateral correlation length of the roughness is larger than the investigated wavelength. If the correlation length becomes smaller than the wavelength, scattering is no longer negligible. When roughness σ is given for one specific interface between two materials of which refractive indices are n_1 and n_2, Fresnel reflectivity and transmissivity are given as follows [91]:

$$
\begin{aligned}
r^*_{l+1R} &= r_{l+1R} \exp\left[-2\left(\tfrac{2\pi\sigma}{\lambda}\right)^2 n_l{}^2\right] \\
r^*_{l+1L} &= r_{l+1L} \exp\left[-2\left(\tfrac{2\pi\sigma}{\lambda}\right)^2 n_{l+1}{}^2\right] \\
t^*_{l+1R} &= t_{l+1R} \exp\left[-\tfrac{1}{2}\left(\tfrac{2\pi\sigma}{\lambda}\right)^2 (n_{l+1}-n_l)^2\right] \\
t^*_{l+1L} &= t_{l+1L} \exp\left[-\tfrac{1}{2}\left(\tfrac{2\pi\sigma}{\lambda}\right)^2 (n_{l+1}-n_l)^2\right]
\end{aligned}
\tag{3.5}
$$

where Fresnel coefficients for the interface with no roughness is given as follows:

$$r_{l+1R} = \frac{n_l - n_{l+1}}{n_l + n_{l+1}}, \quad r_{l+1L} = \frac{n_{l+1} - n_l}{n_l + n_{l+1}}$$

$$t_{l+1R} = \frac{2n_l}{n_l + n_{l+1}}, \quad t_{l+1L} = \frac{2n_{l+1}}{n_l + n_{l+1}} \tag{3.6}$$

Transfer matrix is then written as it gives the Fresnel coefficients,

$$D_l \begin{pmatrix} \alpha & \beta \\ \gamma & \delta \end{pmatrix} D_{l+1} = \frac{1}{t_{l+1R}^*} \begin{pmatrix} 1 & -r_{l+1L}^* \\ r_{l+1R}^* & t_{l+1R}^* t_{l+1L}^* - r_{l+1R}^* r_{l+1L}^* \end{pmatrix} \tag{3.7}$$

which is finally used to calculate the (energy) reflectivity of the rough-interface DBRs. From our experimental results, it is found that nitride DBRs can be made within interface RMS roughness of approximately 4 nm. With this value, reflectivity of 42-period $Al_{0.35}Ga_{0.65}N$/GaN DBR is calculated and compared with experimental results. Figure 3.12 shows simulated reflectivities of the DBRs, both with and without roughness. As for the peak reflectivity, small reduction is expected. When microcavity is grown on these DBRs, reflectivity spectra change drastically in the case of rough interface, as illustrated in Figure 3.13. However, it should be mentioned that these change reflects destructive interference occurred at the topmost interface, i.e., the surface of the DBR, and such situation is only should be considered when one observes as-grown microcavity structures. When top mirror is coated on top of the microcavity, effective reflectivity that light propagating inside the cavity is actually influenced is somehow slightly reduced one such as shown in Figure 3.12.
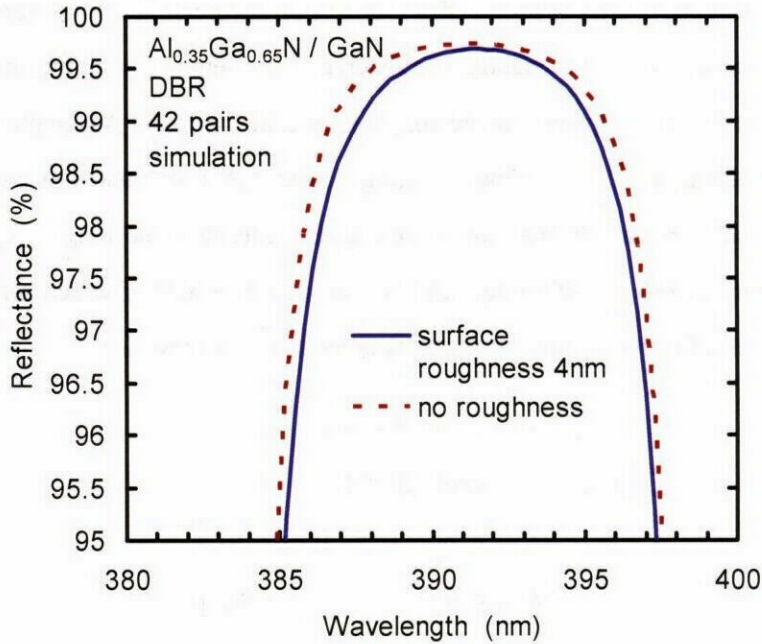

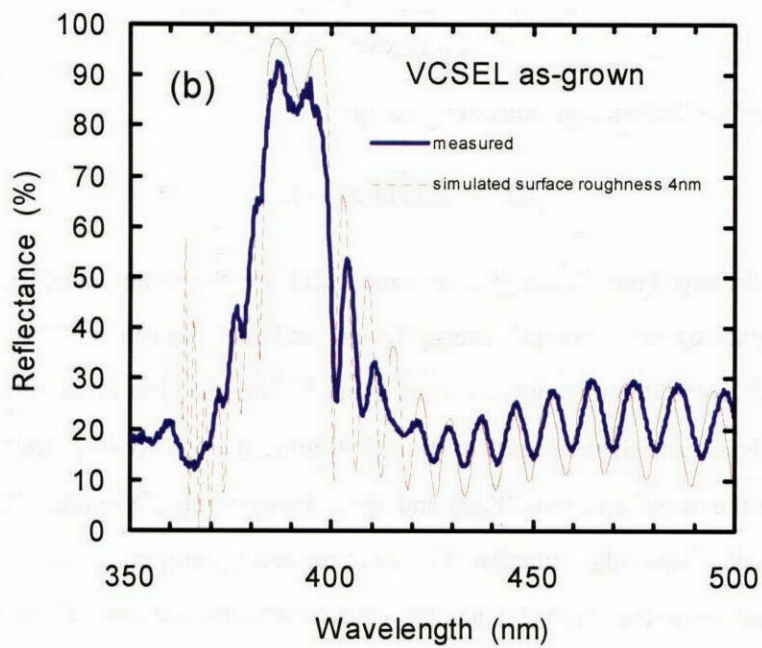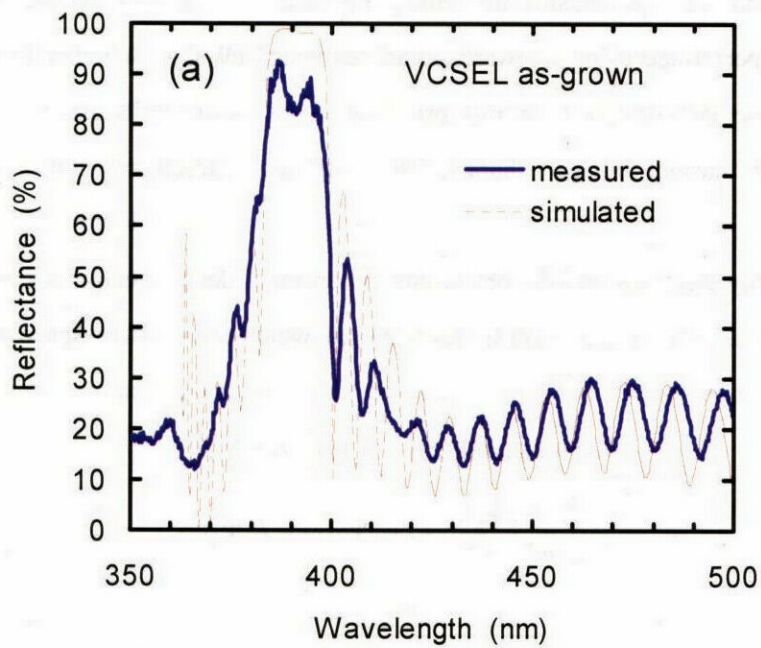Figure 3.12 simulated reflectivity of 42-period DBR with roughness

Figure 3.13 Effects of interface roughness on reflectivity with (a) no roughness (b) σ=4nm

3.6 Theoretical Analysis on Potential and Electrical Conductivity of AlGaN/GaN DBRs

To understand the mechanisms governing electrical conductivity of the nitride n-DBRs, calculations are performed using freeware called nextnano3 (Walter Schottky Institute) [92]. With this software, one can calculate various properties such as potential profiles, carrier density distributions, or current-voltage characteristics of any structures consisting of various semiconductors.

Hereafter, only electrons and donors in one-dimensional device geometries are considered in the following equations. A quasi-Fermi level $E_{Fn}(z)$ which varies over space is taken for the solution of the system.

$$-\operatorname{div}\left[\varepsilon(z)\operatorname{grad}\Phi(z)\right] = -4\pi e\left[-n + N_D^+\right] \tag{3.8}$$

$$-\frac{\hbar^2}{2}\frac{\partial}{\partial z}\frac{1}{m^*}\frac{\partial \Psi_n(z)}{\partial z} + V(z)\Psi_n(z) = E_n\Psi_n(z) \tag{3.9}$$

$$\operatorname{div}(\vec{j}) = 0 \tag{3.10}$$

For the density of the ionized donors, following equation is obtained:

$$N_D^+(z) = \frac{N_D(z)}{1 + g_D \exp\dfrac{E_{Fn}(z) - E_D}{kT}}. \tag{3.11}$$

Starting from the Boltzmann equation one get:

$$j(z) = \mu_n(z)n(z)\frac{\partial}{\partial z}E_{Fn}(z) \tag{3.12}$$

for the current density. Here $N_D(z)$, E_D, g_D, and $\mu_n(z)$ are the donor density, the ionization energy, the degeneracy factor of the energy levels, and the electron mobility, respectively.

Equation (3.8) is the Poisson equation. Here n and N_D^+ are the electron density and the ionized donor density. The 1-band Schrödinger equation (3.9) gives the density of states for the quantized states (that have the wave functions $\Psi_n(z)$ and the corresponding eigenvalues E_n) where $V(z) = E_{c0}(z) - e\Phi(z)$ is the band edge function. The electron density $n(z)$ which goes into the Poisson equation is obtained by occupying the quantized states $\Psi_n(z)$ using the quasi-Fermi level $E_{Fn}(z)$.

$$n(z) = g_{\text{valley}}\frac{m^*(z)kT}{\pi\hbar^2}\sum_n|\Psi_n(z)|^2\ln\left[1 + \exp\left(\frac{-E_n + E_{Fn}(z)}{kT}\right)\right] \tag{3.13}$$

Here, g_{valley} stands for the degeneracy factor of the valley and m^* for the effective mass of the electron.

42

The current continuity equation (3.10) provides the connection between the electron density and the quasi-Fermi level. The self-consistent solution of this system of equations is uniquely determined by the potential $\Phi(z)$ and the quasi-Fermi level $E_{Fn}(z)$.

The actual calculations are divided into two blocks, Poisson block and current block, namely. In Poisson block, the Schrödinger equation (3.9) and the Poisson equation (3.8) are solved self-consistently by a predictor-corrector approach at fixed, space dependent quasi-Fermi level resulting in the new potential and the new quantized states. In current block, the new quasi-Fermi level is obtained by solving the current continuity equation (3.10) at fixed potential and fixed states. Then this cycle will be repeated until self-convergence is reached.

Table 3.1 summarizes parameters used in the calculations.

			GaN	AlN	bowing	Reference
conduction band mass	$m_c{}^*$	$[m_0]$	0.20	0.30	0.0	[93], [94]
conduction band nonparabolicity			0.6	0.0	0.0	
conduction band energy (0K)	E_c	[eV]	2.789	4.712	0.7	[94]
valence band mass (hh)	$m_{hh}{}^*$	$[m_0]$	2.090	10.42	0.0	[95]
valence band mass (lh)	$m_{lh}{}^*$	$[m_0]$	0.740	0.24	0.0	[95]
valence band nonparabolicity			0.015	0.0	0.0	
valence band energy	E_v	[eV]	-0.726	-1.526	0.0	[96]
varshni parameters alpha	α	[eV/K]	$0.909{\times}10^{-3}$	$1.799{\times}10^{-3}$	0.0	[93], [94]
varshni parameters beta	β	[K]	830	1462	0.0	[93], [94]
static dielectric constant	ε_0		9.8	9.567	0.0	[97]
optical dielectric constant	ε_{inf}		5.47	4.84	0.0	[98]
uniaxial vb deformation potential	D_1	[eV]	-3.7	-17.1	0.0	[93], [94]
	D_2	[eV]	4.5	7.9	0.0	[93], [94]
	D_3	[eV]	8.2	8.8	0.0	[93], [94]
	D_4	[eV]	-4.1	-3.9	0.0	[93], [94]
	D_5	[eV]	-4.0	-3.4	0.0	[93], [94]
	D_6	[eV]	-5.5	-3.4	0.0	[93], [94]
lattice constants (300K)	a	[nm]	0.3189	0.3112	0.0	[93], [94], [99]
	c	[nm]	0.5185	0.4982	0.0	[93], [94], [99]
lattice constants temp. coefficient	a	[nm/K]	$5.59{\times}10^{-6}$	$4.15{\times}10^{-6}$	0.0	[100], [101]
	c	[nm/K]	$3.17{\times}10^{-6}$	$5.27{\times}10^{-6}$	0.0	[100], [101]
piezoelectric constants	e_{33}	$[C/m^2]$	1.27	1.79	0.0	[93]
	e_{31}	$[C/m^2]$	-0.35	-0.50	0.0	[93]
	e_{15}	$[C/m^2]$	-0.30	-0.48	0.0	[97]
elastic constants	C_{11}		390	396	0.0	[93], [94]
	C_{12}		145	137	0.0	[93], [94]
	C_{13}		106	108	0.0	[93], [94]
	C_{33}		398	373	0.0	[93], [94]
	C_{44}		105	116	0.0	[93], [94]

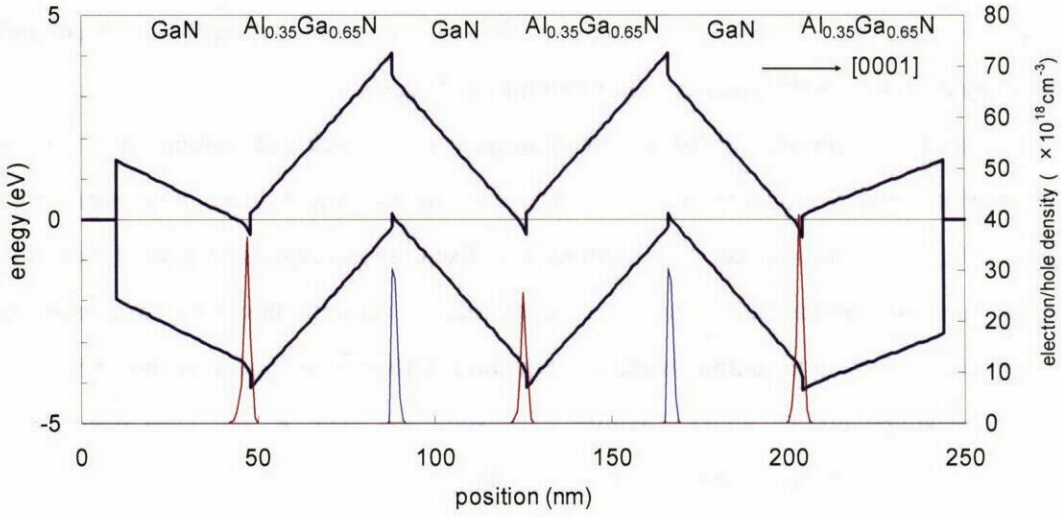Table 3.1 Material parameters of nitride semiconductors used in the calculations

Figure 3.14 Energy band edges and electron/hole densities of a nondoped DBR

First, potential profiles of nondoped $Al_{0.35}Ga_{0.65}N$ (40nm) / GaN (38nm) DBRs are investigated. A 3-period DBR in which the two boundaries are terminated with schottky contacts (barrier height 1.46 eV: corresponds to Al) is considered. In fig. 3.14, the calculated energy band edges, electron density and hole density are illustrated in the thick line, the red line, and the blue line, respectively. It can be seen that the density of the current flowing across the DBR is negligible because of the high energy barriers in nondoped DBRs. No tunneling through the barriers can be expected either, although there appear parasitic hole channels at each GaN on $Al_{0.35}Ga_{0.65}N$ interface [102].

Next, the band edge positions and the electron density are calculated for DBRs in which Si is uniformly doped. The activation energy of Si is assumed to be 30 meV for both GaN and AlGaN. In the case of doping concentrations of 1.0×10^{18} cm^{-3} (GaN) and 5.0×10^{18} cm^{-3} (AlGaN), results are shown in Fig. 3.15. These doping concentrations correspond to the carrier densities of the fabricated DBR if the activation is assumed to be perfect. Again, little current flows across the DBR since the energy barrier is still high. The calculated results for a highly-doped condition, where the doping concentration is increased ten times higher than the previous case, are shown in Fig. 3.16. This doped DBR may exhibit an asymmetric, rectifying behavior in the current-voltage characteristics, considering the shape of the energy barrier similar as that of a Schottky barrier.
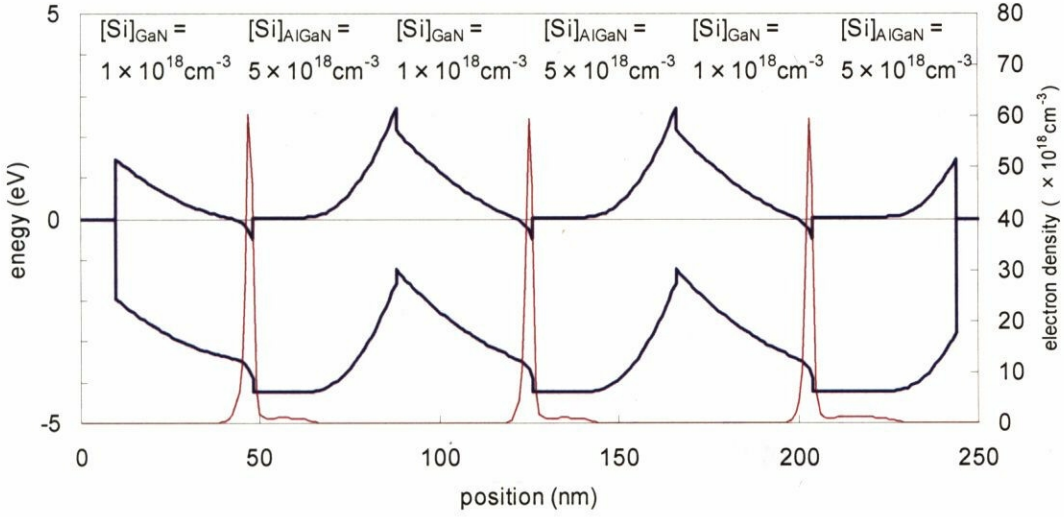
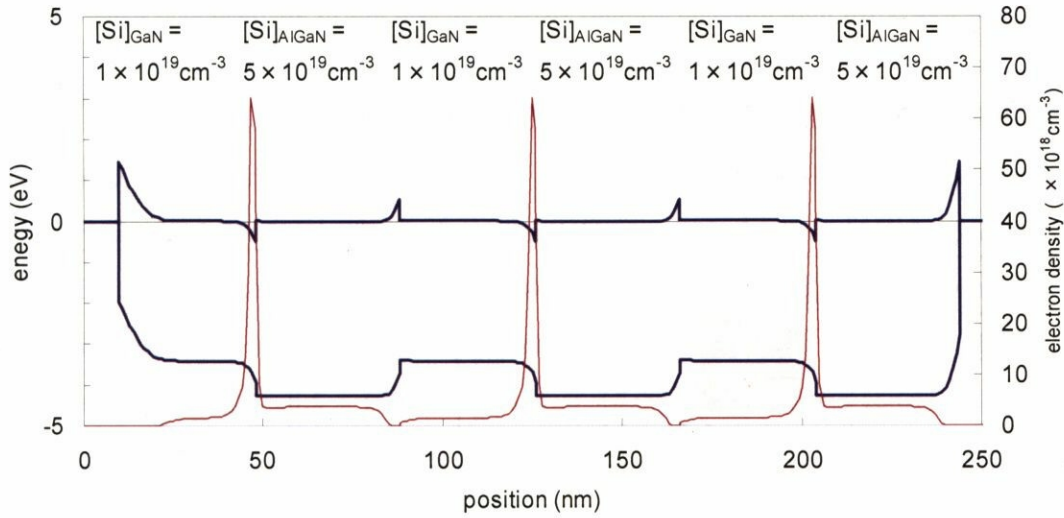Figure 3.15 Energy band edges and electron density of a Si-doped DBR (n $\sim 10^{18}$ cm^{-3})

Fig. 3.16 Energy band edges and electron density of a Si highly-doped DBR (n $\sim 10^{19}$ cm^{-3})

Experimentally, DBRs in which n-AlGaN/n-GaN superlattice layers were used instead of n-AlGaN layers were also fabricated. The energy band edges and the electron density distribution for a Si-doped superlattice DBR (Structure: [Al$_{0.44}$Ga$_{0.56}$N (2.0nm) / GaN (0.5nm)]$_{16}$ / GaN (38nm)),

45

where the two ends are terminated with ohmic contacts, are shown in Fig. 3.17. In this case, the doping concentrations in GaN and superalttice are similar as in the case of Fig. 3.15. The expected conductivity is also similar though the modulated potential at the superlattice modifies the electron distribution.
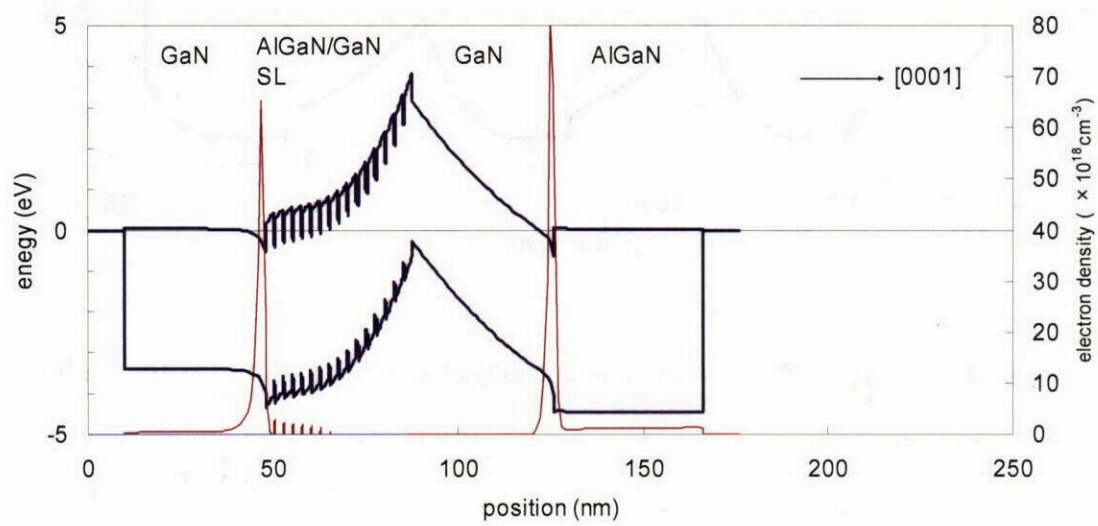

Fig. 3.17 Energy band edges and electron density of a Si-doped superlattice DBR (n $\sim 10^{18}$ cm^{-3})
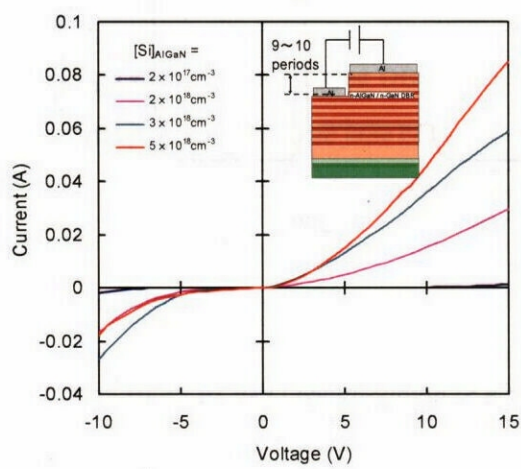

Fig. 3.18 Room temperature current-voltage characteristics of Si-doped DBRs
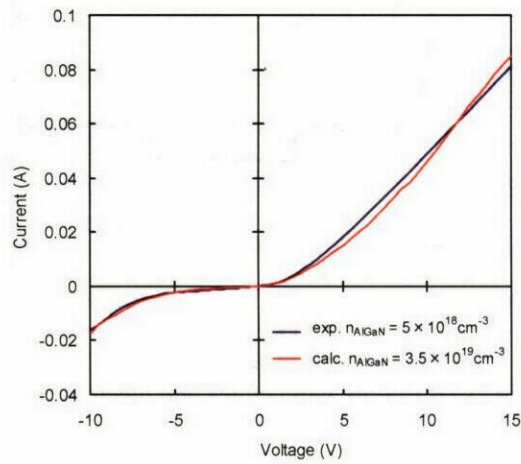
Fig. 3.19 Comparison between calculated and measured I-V characteristics of Si-doped DBRs

We investigated electrical characteristics of the fabricated n-DBRs (without superlattices). As plotted in Fig. 3.18, the current-voltage characteristics measured at room temperature showed a rectifying behavior. The polarity of the applied voltage is defined such that a positive bias corresponds to a situation when a cathode is on the surface side ([0001] direction). In the experiment, n-DBRs of around 10 periods were etched by using Cl_2/Xe RIE, and Al electrodes were evaporated on both the original and the etched surfaces. It can be seen form the figure that higher doping concentrations gave higher current densities for the positive bias. When the doping concentration is $[Si]_{AlGaN} = 5 \times 10^{18}$ cm^{-2}, the series resistance for the positive bias condition is on the order of 100 Ω. Considering the area of the mesa where the current flows is approximately 37,000 μm^2, the resistivity of this DBR is on the order of 1 $\Omega \cdot m$.

As shown in Fig. 3.15, a normal current transport mechanism in which free electrons move in the conduction band is negligible for this doping concentration. Therefore, in order to study the origin of this discrepancy, the electrical characteristics of n-DBRs are calculated. In Fig. 3.19, the calculated and the measured current-voltage characteristics are compared. In this figure, the current-voltage characteristic of the measured DBR (doping concentration $[Si]_{AlGaN} \cong n_{AlGaN} = 5 \times 10^{18}$ cm^{-3}) is compared to that of an n-DBR with additional parallel and series resistances. At first, assuming the doping concentration of $n_{AlGaN} = 5 \times 10^{18}$ cm^{-3}, the simulation have revealed that a resistance of the n-AlGaN/n-GaN periodic heterojuncitons is really high, indicating the moderately-doped DBR is practically insulating. On the other hand, electrical conductivity is calculated to be expected when the doping concentrations increase. Then we performed several calculations with different doping concentrations. When assuming relatively high doping concentrations of $n_{AlGaN} = 3.5 \times 10^{19}$ cm^{-3} and $n_{GaN} = 7.0 \times 10^{18}$ cm^{-3}, and considering the series resistance of $R_s = 140$ Ω and the parallel resistance of $R_p = 2$ kΩ, the calculated I-V curve gives a good agreement with the experimental data.

The experimentally obtained rectifying properties can be explained from the asymmetric shape of the potential barrier at the GaN on AlGaN interfaces, as shown in Fig. 3.16. The rectifying characteristics similar as that of a Schottky barrier can be expected. The effective barrier height that electrons must overflow is dependent on the polarity of the applied bias: if the bias is negative, the barrier height is higher than the case of positive bias. Actually, such tendency is calculated and agrees well with the experimental results as shown in Fig. 3.19.

As mentioned above, the experimental data for the n-DBR with carrier concentrations of n_{AlGaN}

$\cong$ [Si]$_{AlGaN}$ = 5 × 10^{18} cm^{-3} shows rectifying, conductive characteristics similar as the simulated result of the highly-doped DBR in which doping concentrations are about one order of magnitude higher than the measured values. One may think there is a possibility that the effective free electron concentrations are higher than the experimentally-obtained values. The carrier density in n-GaN layers was obtained by Hall measurements of the bulk samples. For n-AlGaN, the carrier density was estimated assuming that the measured carrier density of n-DBRs by Van der Pauw configuration simply consist of equivalent contributions from the carrier densities of both n-GaN and n-AlGaN layers. The carrier density in n-AlGaN was obtained by subtracting corresponding n-GaN carriers from the measured carrier density of n-DBRs. Hall measurements of n-AlGaN bulk layer samples were not possible because the bulk n-AlGaN had been difficult to grow. There is a possibility that only a few periods of the DBR layers just beneath the contact is measured by the Hall measurement, resulting in the errors. It is therefore important to measure the accurate doping concentrations by SIMS or other probing techniques. Carrier density distributions can also be deduced from the measured capacitance–voltage characteristics.

There might arise a question about the reasonability of the analyzed values of the additional parallel and series resistances considered in the calculations of the current-voltage characteristics. Generally, the resistivity of as-deposited Al contact on n-GaN can be on the order of 10^3 ~ 10^4 Ωcm^2. The small contact pads fabricated in this experiment have the area of 2.5 × 10^{-5} cm^2. Considering that RIE can easily induce defects on the etched surfaces and deteriorate the electrical properties of them, contact resistance of several tens of Ohms may be obtained when the fabrication processes are not optimized. In addition, lateral conduction paths between the two electrodes must have some resistance. Considerable part of the deduced series resistance of 140 Ω can be attributed to such resistances. On the other hand, the existence of the parallel resistance strongly suggests that there are some leak paths or parasitic conduction paths beside the predicted transport mechanism of the n-DBR. Such conduction paths are most probably attributable to the structural defects, such as threading dislocations. The semi-empirically deduced parallel resistance of 2kΩ seems relatively small for the leakage resistance, implying that further improvement is expected for the quality of the DBRs. It is essential to optimize the conditions of both MOCVD growth and device fabrication processes.

Resistivity of n-DBRs could be lowered by nearly half by introducing the superlattice. The supelattice DBRs are attractive since they can reduce the resistivity while maintaining the optical

characteristics. Since the theoretically predicted contributions of the superlattice is small if the doping concentrations are on the order of 10^{18} cm^{-3}, it is suggested that one should consider the possibility of underestimated carrier concentrations as described above to explain the experimental results. On the other hand, currents passing though the interface states may increase as AlGaN/GaN interfaces increase in the superlattice.

Ive et al. reported that they could observe the current flowing across a Si-doped AlN/GaN DBRs [89, 103]. They confirmed by using surface potential measurements that the current did not result from the threading dislocations and mentioned the possibility that the effective barrier height could be lowered since the interface states located at the AlN/GaN interface might compensate the internal electric fields. However, since in order to fully compensate the internal fields one needs the interface charges with density as high as $\sim 10^{13}$ cm^{-2}, the effects of the interface charges are not decisive even if the proposed mechanism actually works. On the other hand, a hypothesis that the current flowing across the n-DBRs are mainly attributed to the impurity band conduction can also be considered. Moon et al. mentioned the results of Ive et al. in the context of an explanation for their experimental results on the low-temperature electrical conductivity of GaN deposited on Si$_x$N [104]. They assumed a model in which a degenerated impurity band exists in the highly Si-doped GaN (or AlN) and the free electron at the low temperature results from the metallic-like nature of the doped GaN. The electrical conductivity of this model may be explained by the hopping conduction between the impurity states (or bands). The interface states around the AlGaN/GaN interface, possibly locating deeply inside the energy band gap, can be one of the candidates of other deep states than the Si-related impurity band.

Nevertheless, it is concluded that the electrical conductivity in nitride DBRs is really obtainable when both high quality and high doping concentrations are achieved. Recently, crystal growth techniques for AlN or AlGaN materials have been greatly improved as the researches on UV light emitting devices progress. For example, alternative supply (or pulse supply) method where source gases are supplied alternatively is proved to be effective to reduce the threading dislocation density in AlN [105]. Therefore, it is expected that high-quality electrically-conductive nitride DBRs can be grown by utilizing such techniques.

3.7 Summary

In this chapter, growth and characterization of nitride DBRs with both high reflectivity and

reasonable conductivity was described. Si doping was done to obtain n-type AlGaN/GaN DBR and it was revealed that an optimum doping concentration existed, in terms of reflectivity. Also, doping concentration in n-AlGaN layers could be higher than n-GaN layers while maintaining high reflectivity. For further improvement of electrical characteristics as well as structural quality, superlattice was introduced into n-AlGaN/n-GaN DBRs. It has been shown that AlGaN/GaN superlattice efficiently suppress cracking in the heterostructure. XRD measurements revealed that AlGaN and GaN were grown pseudomorphically throughout the DBR structure, which resulted in the thicker critical thickness of the superlattice DBR. Reasonably high reflectivity of 94.5 % was obtained with the 26-pair SL-DBR. Finally, DBRs of which reflectivity exceeds 99% have been successfully grown. Also Si doping was demonstrated in the high-reflectivity DBR. For VCSEL applications, higher reflectivity is crucial to take expected advantages such as lower threshold current density. Theoretical analyses have been performed to shed light on the origin of the electrical conductivity of the n-DBRs. It is suggested that electrically conductive nitride DBRs is really available when both high quality and high doping concentrations are achieved. These results will propel the development of current-injected nitride VCSELs.